Available online at www.sciencedirect.com
SCIENCE DIRECT®
Earth and Planetary Science Letters 243 (2006) 594–606
EPSL
www.elsevier.com/locate/epsl

A case history of paroxysmal explosion at Stromboli: Timing and dynamics of the April 5, 2003 event

M. Rosi [a], A. Bertagnini [b], A.J.L. Harris [c], L. Pioli [a,*], M. Pistolesi [a], M. Ripepe [d]

[a] *Dipartimento di Scienze della Terra, Università di Pisa v. S. Maria 53 56126 Pisa, Italy*
[b] *INGV, Pisa v. Della Faggiola 32 56100 Pisa, Italy*
[c] *HIGP/SOEST, University of Hawaii, 1680 East-West Road, Honolulu, HI 6822, USA*
[d] *Dipartimento di Scienze della Terra, Università di Firenze, v. La Pira 4 50121 Firenze, Italy*

Received 26 October 2005; received in revised form 5 January 2006; accepted 16 January 2006
Available online 21 February 2006
Editor: V. Courtillot

Abstract

On April 5, 2003, Stromboli volcano (Italy) produced the most violent explosion of the past 50 years. The event was exceptionally well documented thanks to the presence on the island of several scientists and a large number of instruments deployed over the preceding months to monitor the effusive eruption that began in December 2002. Integration of visual documentation, deposit features and geophysical data allowed an accurate reconstruction of the explosive event and its dynamics. The eruption consisted of a 8-min long explosive event which evolved through four phases whose timing was precisely recorded by an infrared thermometer located about 450 m from the summit crater. Phases 2 and 3 lasted 39 and 42 s, respectively. Both had an impulsive character, were responsible for ejecting almost the entire mass of the pyroclastic products. Phases 1 and 4 represented, respectively, a short-lived precursory event and a waning tale. During Phase 2, meter-sized ballistic blocks were launched with velocities of 170 m/s to altitudes of up to 1400 m above the craters. These fell on the volcano flanks and on the village of Ginostra, about 2 km distant from the vent. A vertical jet rose above the craters which developed to feed a convective plume that reached a height of up to 4 km. The calculated mass of the Phase 2 fallout deposit and mass discharge rate were $1.1–1.4\times10^8$ kg and $2.8–3.6\times10^6$ kg/s, respectively. During Phase 3 a scoria flow deposit, with an estimated volume of $0.9–1.1\times10^4$ m^3, was erupted from the same vent that fed the ongoing sustained lava flow. The average mass discharge rate for this phase was $2.5–3.1\times10^5$ kg/s.

Products emitted during Phases 2 and 3 consisted of lithic and fresh magmatic material in similar proportions. The juvenile fraction consisted of a deep-originated, almost aphyric, highly vesicular pumice mingled with a shallow-derived, crystal-rich, moderately vesicular scoria.

Similarities with the eruption dynamics of other historical paroxysms at Stromboli makes the April 5, 2003 explosion representative of these highly energetic events that constitute the most hazardous volcanic phenomena at Stromboli volcano.

Keywords: stromboli; Thermal monitoring; paroxysm; explosive dynamics; ballistic ejecta

* Corresponding author.
E-mail address: pioli@dst.unipi.it (L. Pioli).

0012-821X/$ - see front matter © 2006 Elsevier B.V. All rights reserved.
doi:10.1016/j.epsl.2006.01.035

1. Introduction

Stromboli island, located in the Tyrrhenian Sea 60 km north of Sicily (Fig. 1), is a 924 m high volcanic cone, which rises from a depth of 1500–2000 m below sea level. The most prominent feature of the island is the Sciara del Fuoco, a horseshoe-shaped depression bounded by steep cliffs hundreds of meters high, which formed as a result of a series of slope failures [1]. The current activity of Stromboli has likely persisted since the IV–VII century AD. Activity has been dominated, at least over the last two centuries, by low-energy, Strombolian explosions that usually occur at intervals of 10–20 min from vents within an elliptical, SW–NE elongated, crater area located at an elevation of 700 m [2] (Fig. 1). The persistent activity is accompanied at intervals of years by lava flow emission onto the Sciara del Fuoco. Strombolian explosions and lava flows are fed by a crystal-rich HK basalt, probably residing in the shallow part of the magmatic system. This normal activity is occasionally broken by discrete, violent explosions called 'paroxysms' [3]. These consist of explosive events of several minutes in duration that launch blocks up to 2–3 km from the source, damaging the settled area, and feed a vertical column of gas and pumice extending to several kilometers in height [4,5]. These events occur suddenly, during persistent mild activity and appear not to be preceded by any anomalous activity or instrumental precursors. Because of their violent and unpredictable nature, paroxysms represent a major threat to people either visiting the volcano summit or living in the settled areas.

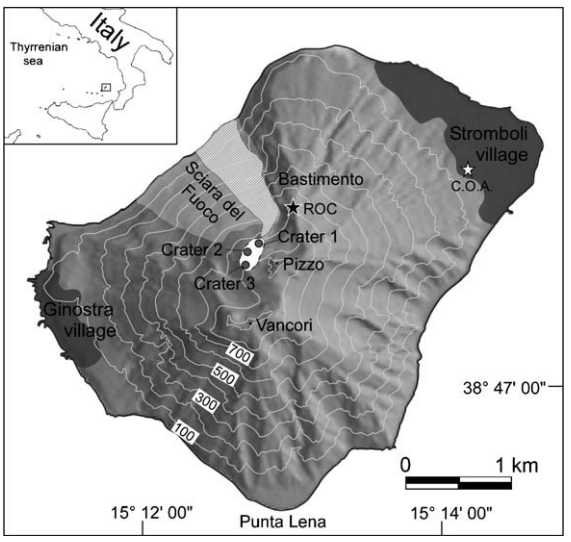

Fig. 1. Map of Stromboli Island. White zone: summit crater area; striped zone: 2002–2003 lava flow field; black star: location of IR thermal station (ROC); white star: location of Italian Civil Protection Center (COA).

On April 5, 2003, at 9:13 local time (7:13 GMT), a paroxysmal eruption occurred while an effusive eruption was in progress. At that time the Italian Civil Protection and scientific personnel were present on the island to handle and monitor the eruptive crisis. The paroxysm was observed, photographed and filmed by several researchers. In addition to visual observations, instruments deployed in the preceding months provided an unprecedented geophysical and geochemical record that could be applied to fully document and understand the paroxysmal event. In this paper we analyze the visual documentation of the event and assess the time correlations with thermal radiometer, seismic and acoustic records to precisely track the progression of the different eruptive phases. Accurate field analysis of pyroclastic deposits carried out shortly after the paroxysm are added to further constrain the event and to make inferences regarding the origins of the different eruptive phenomena and to assess the physical volcanology of the event. Integration of all data sets provides a compelling quantitative reconstruction that sheds new light on the intimate dynamics of these events.

2. The 2002–2003 eruptive crisis and the paroxysmal explosion of April 5, 2003

The 2002–2003 eruptive crisis of Stromboli began in the late afternoon of December 28, 2002, when lava flows were generated by vents opening in the NNE sector of the Sciara del Fuoco and from the crater area (crater 1, Fig. 1). The onset of the lava emission was accompanied by a substantial destabilization and seawards displacement of the Sciara del Fuoco and the generation of moderate scale avalanches of dry volcanic debris [6]. On December 30, 2002 the lava emission and concurrent slope movements culminated in a catastrophic slide that involved both subaqueous and subaerial parts of the Sciara del Fuoco [7]. The slide led to the formation of tsunami waves that caused extensive damage to the village of Stromboli along the northeastern coast of the island [8]. A drop in the magma level within the central conduit, produced by the opening of vents at 500 m a.s.l., also resulted in the collapse of the summit craters and the temporary cessation of the usual mild explosive activity [9].

On April 5, with lava emission still in progress from vents located at 600 m a.s.l. and the summit craters clogged with debris, a paroxysmal explosion occurred. The paroxysm was accompanied by a cannon-like detonation and the formation of a compressive wave

that broke windows in the village of Ginostra, about 2 km distant from the crater area. Blocks launched during the explosion also fell on the NE and SW sectors of the mountain, reaching Ginostra.

The paroxysm was not preceded by any well-recognized precursors. Eye witnesses refer to an explosion at crater 3 (Fig. 1) ejecting hot blocks on April 3; this was eventually considered to have heralded the main explosion [10]. Examination of geochemical data made in the weeks after the event also revealed: (i) lowering in pH values and an increase in H_2 and He in thermal wells located in the eastern part of the Stromboli village starting a couple of weeks before the event [11] and (ii) an increase (up to 4–8 times) in the SO_2/HCl molar ratio measured in the gas plume released from the summit craters, beginning 40–60 h before the event [12]. About 30 s before the eruption a significant deformation was recorded by two continuous GPS stations located near the craters [13].

3. Data collection

Our reconstruction of the April 5 paroxysm uses three types of data: direct visual observations (including photographs and video), post-eruption field surveys (deposit mapping and sampling), and geophysical measurements (thermal, infrasound and seismic).

3.1. Visual observation

Visual data included direct observations of the eruption by two of the authors, who were stationed at the COA (Centro Operativo Avanzato, Fig. 1) ~2 km from and 600 m below the erupting vents. In addition, we gathered pictures taken by various individuals who kindly made their data available. Pictures of the event were taken from sites located at different elevations and azimuths around the northeastern part of the island. Of particular value were two data sets. First, P. Scarlato (INGV) shot, from the COA, a video starting about 1 min after the onset of the event and lasting for about 7 min. The most complete visual documentation of the eruption was taken with digital and thermal cameras by S. Calvari and L. Lodato (INGV), during a helicopter over-flight of the active lava flow field and crater area before, during and after the paroxysm [10]. Unfortunately no images where taken from the western side of the island (Ginostra village, Fig. 1).

Estimation of approximate durations of the eruptive sequence was made using the relative timing of the S. Calvari pictures as recorded by the internal clock of the digital camera.

3.2. Geophysical monitoring

An integrated geophysical monitoring system consisting of three thermal infrared (IR) thermometers, a 5-element infrasound array, a further 4 pressure sensors co-located with the IR-thermometers and 4 broadband seismometers was deployed by the Department of Earth Sciences of the University of Firenze around the summit craters from January 2003 [14,15]. As of April 2003 a 15° field of view (FOV) IR-thermometer had been installed about 450 m NE of the crater 1 at Bastimento (Fig. 1) [15]. Although the pressure sensors recorded the acoustic signal at the onset of the eruption, all the sensors were destroyed within the first 50 s. The seismometers also recorded the onset of the eruption, as well as a signal consistent with the sensor moving when a large block landed near the station. Data, though, were generally saturated. The IR-thermometer, however, recorded good, unsaturated data throughout the eruption. Thus the peaks in the thermal log record due to the passage of bursts of hot material rising through the instrument FOV could be used to detail and time various events. Photographic evidence reveals that the FOV would have been filled with an opaque, ash-rich plume, with an emissivity of ~0.95 [16]. Therefore the arrival of a plume at a relatively high temperature (compared with the cold background comprising sky plus cold crater wall) and subsequent pulses of ejected material at different temperatures will cause oscillations in the signal. However, because the atmospheric conditions would have been extremely poor during the eruption, we do not trust in any way the absolute value of the thermal signal and any retrieved temperatures will be much lower than the maximum temperature of the plume itself. Thus we focus on trends in the relative signal, and the rate at which the signal changed.

3.3. Field survey and deposit analyses

An initial inspection of the deposits was made just a few hours after the eruption by one of us (M. Rosi). Sample collection and mapping across the distal and proximal areas were completed within a few weeks and a few months, respectively. During fieldwork we mapped distribution, thickness and mass/unit area of the fallout deposit. Selected sampling was carried out for grainsize, componentry and petrographic observation of both juvenile and lithic fragments.

In addition, analysis and comparison of images obtained during aerial photogrammetry surveys made about one month before and a few days after the eruption were kindly made available by M. Marsella

(University of Roma 3) [17]. These were used to map impact craters formed by ballistic fallout of blocks on the volcano flanks.

4. Results

From an examination of the visual documentation, geophysical data and deposit analysis we defined three main energetic phases. Each could be distinguished by their differing character and style of emission. These were preceded by a less vigorous opening phase and are summarized as follows:

Phase 1: eruption onset.
Phase 2: climactic explosion.
Phase 3: pyroclastic flow and smaller explosions.
Phase 4: terminating ash explosions.

4.1. Visual description of the explosion

4.1.1. Phase 1

Images taken from the helicopter a few minutes before the onset of the paroxysm, indicate that there was no visible variation in lava emission [10]. At that time a white (heavily condensed) plume, typical of the persistent gas emission from Stromboli's active vents during bad weather, was apparent being blown to the SW in strong winds and mixing with atmospheric clouds. The eruption began with a relatively weak emission of red ash to a height of a few tens of meters which mixed with the gas plume. This emission started at craters 2 and 3, and can first be observed in the images as a slight reddening of the plume above these two craters. After about 19 s the emission became more intense and spread to crater 1 (Fig. 2a). The ash emission was swiftly consumed by two highly energetic plumes ~30 s after phase 1 began.

4.1.2. Phase 2

The second phase began with the emission of a rapidly expanding, billowing, dark-colored ash plume that was, seconds later, over taken by a second plume composed of multiple jets, comprising leading blocks with ashy contrails of lighter grey ash (Fig. 2b). Visual observations from the helicopter indicate that the explosion involved simultaneously both craters 1 and 3 [10].

The convective plume drifted southwards with the wind and was observed and photographed from the Civil Protection plane flying from Rome to Reggio Calabria by R. Scandone. The pilot estimated a plume height of 4 km above the summit of the volcano (R. Scandone, personal communication). In a picture taken about 50 s after the eruption onset impacts from blocks were clearly visible down to 400–600 m a.s.l. on the NE flank of the cone. In addition, intense bomb fallout was marked by the presence of a continuous, dark curtain around the column (Fig. 2c).

4.1.3. Phase 3

Forty-nine seconds after the eruption onset two ground-hugging, light-grey colored ash plumes propagating laterally and vertically between the crater area and the Bastimento ridge were visible in front of the main column on pictures taken from the NE (Fig. 2c). This developed into a pair of phoenix clouds that rose convectively (Fig. 2d).

Around 105 s after the paroxysm began, a light grey vapor-dominated cloud was visible at the base of the phoenix clouds (Fig. 2e). Successive pictures taken by S. Calvari from the helicopter hovering in front of the Sciara del Fuoco about 3 min after the event began reveal that the vapor originated from the lava field and from the slope south of the lava field (Fig. 2f). By this time, a series of small explosions at the summit vents are recognizable in the movie recorded from COA.

4.1.4. Phase 4

Phase 4 began about 3 min after the onset of the paroxysm and consisted of a series of small explosions from craters 2 and 3. These explosions emitted red colored, ash-laden plumes that reached a maximum height of about 600 m before drifting south (Fig. 2f).

4.2. Geophysical data

The thermal record displays several discrete peaks, revealing that no sustained high-temperature phases occurred during the eruption. Instead the eruption consisted of a series of discrete bursts, each of which could be grouped, on the basis of burst onset time and amplitude, into the same four eruption phases as identified from the observational data.

The explosion was first evident in the IR-thermometer data as a low amplitude oscillation beginning at 7:13:07 GMT. This oscillation developed and decayed relatively slowly, rising to a peak of 27 °C over 4.4 s and lasting ~12 s (Fig. 3). This initial thermal event is interpreted as the phase 1 emission of gas, condensed water vapor and particles (mostly ash), forming an ash-rich plume in the seconds before the main explosion.

The Phase 1 thermal signal was abruptly terminated by a high amplitude thermal event with an impulsive onset, during which temperature increased sharply to 52 °C in

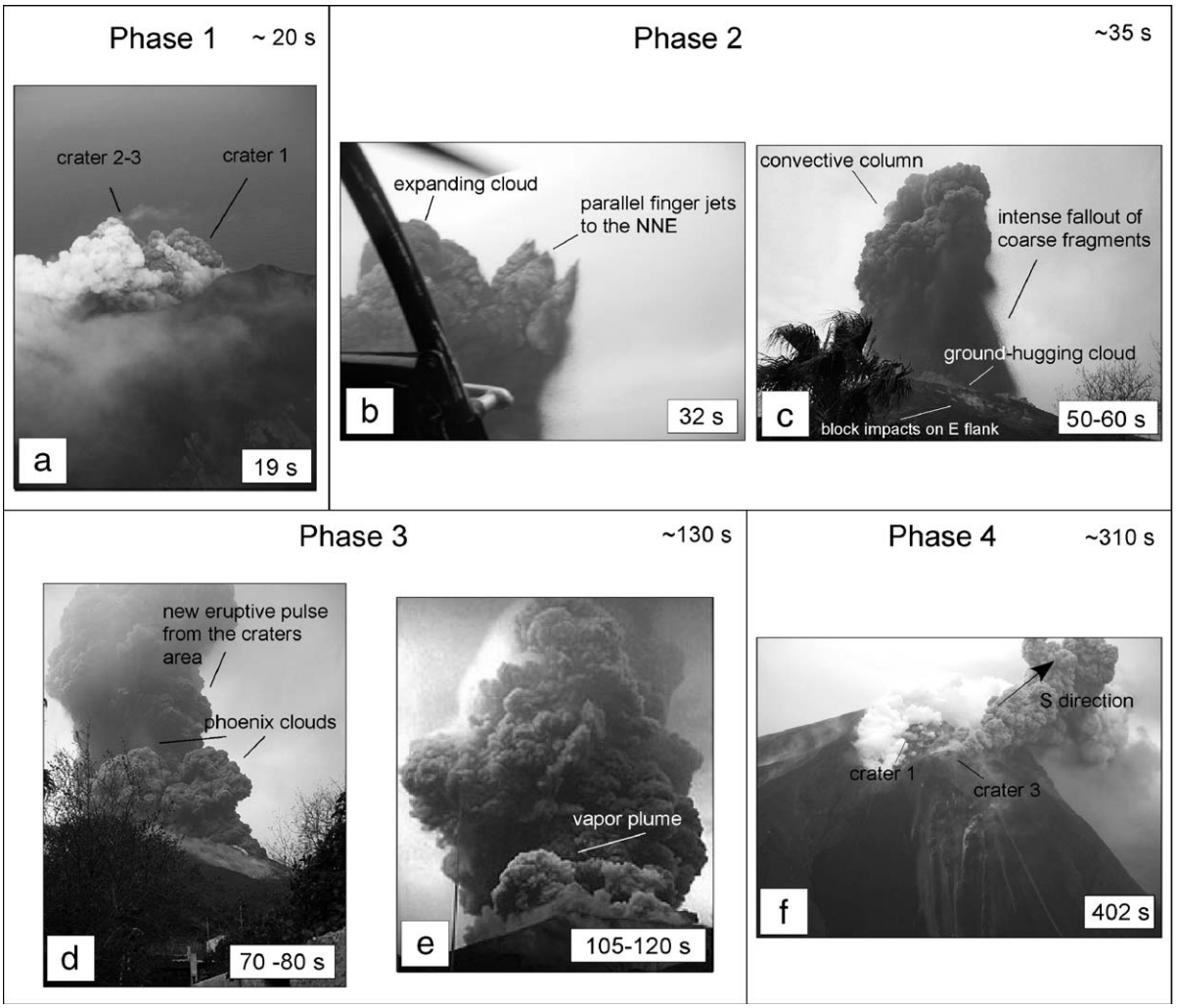

Fig. 2. Pictures of the April 5 eruption. (a) Red ash plume emitted from crater 3 during late Phase 1. (b) Main blast showing ballistic blocks ejected to the NNE and expanding ash cloud during early Phase 2. (c) Vertical column rising above the crater area and formation of pyroclastic flow during early Phase 3. (d) Phoenix clouds rising above the Bastimento area. (e) Vapor plume replacing the phoenix cloud during late Phase 3. (f) Vapor plume and ash plumes emitted from crater 3 during late Phase 4. Pictures in a, b, and f are from S. Calvari in [10], times in the lower right indicate relative times as recorded by digital camera; picture c is from A. Franssen, and pictures d and e are from S. Ballarò.

0.4 s, reaching a peak of 259 °C after 11 s (Fig. 3). This signal can be related to the impulsive ash emission during Phase 2. Following the initial peak the signal began to decay over a period of 28 s to a low of 32 °C. As already stated, due to poor viewing conditions we do not trust the absolute value of the true maximum and would have been complicated by extremely variable line-of sight conditions. The relative signal, though, reveals a decaying limb gave the Phase 2 thermal record an asymmetrical form. This was, however, interrupted by a further three thermal spikes (Fig. 3). We continue to give the raw temperature values to provide a rough measure of the relative thermal intensity of each event.

During Phase 2 the IR-thermometer field of view would have been dominated by activity at crater 1. Thermal activity at other craters would have been obscured by the optically thick ash plume being emitted from crater 1. We interpret the signal in terms of emission of expanding ash plumes (to give the longer onset events) and faster moving blocks (to give the shorter onset events).

A new cluster of thermal spikes of lower amplitude (maximum of 52 °C) and moderate onset times (0.7–1.4 s) followed Phase 2 (Fig. 3). This cluster comprised six spikes all of similar amplitude (37–52 °C) and lasted ~25 s. We interpret this signal as being related to the

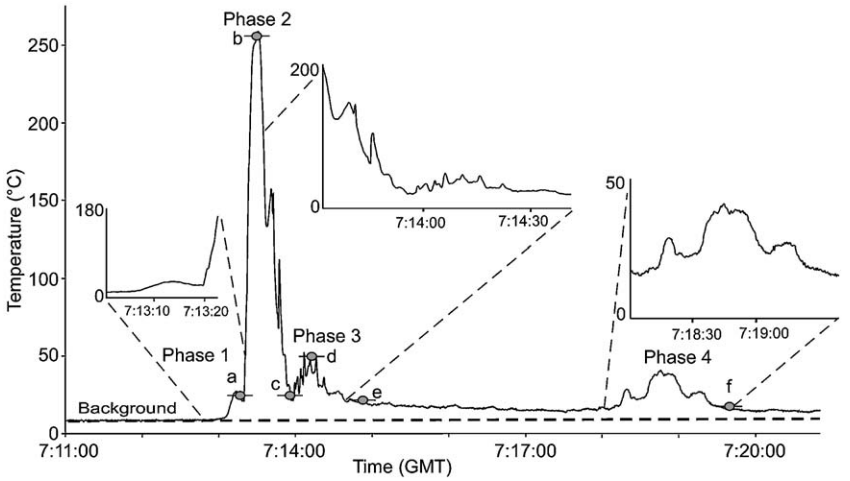

Fig. 3. Temperatures recorded by the IR-thermometer located on the Bastimento ridge during the April 5 eruption at Stromboli. Eruptive phases are defined as indicated in the main text. Background level was defined on the basis of average temperature before the eruption. Letters indicate acquisition points of photographs given in Fig. 2.

pyroclastic flow activity of Phase 3. The phoenix plume rose between the thermometer and crater 1 and would thus have obscured the crater 1 activity from our view; the ash plume itself becoming the source of thermal emission during phase 3.

This was followed by a ~225-s long period of oscillating thermal signal characterized by a series of 13 low amplitude (16–27 °C) thermal events with relatively long (1–11 s) onsets (Fig. 3). From the photographic and video record we know that, by this point, activity at crater 1 had died out and the plume had cleared. Instead the activity had shifted to craters 2 and 3.

Thermally, Phase 4 was terminated by three thermal pulses of moderate amplitude (27–41 °C) and onset duration (2.6–4.7 s). These began at 07:18:13 GMT and lasted 1 min and 27 s (Fig. 3). The photographic and video records show on-going activity at crater 3 at this time, with a major event apparent about 310 s after the eruption began (Fig. 2f). Thus we interpret this part of the thermal signal as relating to this final, major emission from crater 3 which, with the decay of activity at craters 1 and 2, was now visible to the thermal sensor.

Further minor pulses continued for a further 2.5 min, where two low amplitude (~16 °C) thermal oscillations with long onsets (5–6 s) were recorded in the thermal data at 7:20:13 and 7:20:54 GMT, respectively.

4.3. Deposits of the eruption

The deposits that accumulated on the island mainly consist of coarse-to-very-coarse pyroclasts (bombs and blocks) with subordinate amounts of fine ash. Pumice was observed floating in the sea south of the island immediately after the explosion. This was washed ashore on the southern cost of Stromboli and in the Ginostra harbor in the hours following the event.

Four categories of primary deposits can be thus identified: (a) ballistic fallout, (b) fallout tephra, (c) pyroclastic flow, and (d) late ash and lapilli fallout.

4.3.1. Ballistic fallout

Angular blocks (diameter ≤ 5 m) fell all around the summit area, reaching distances of up to 2 km from the vents and often forming large impact craters. Blocks falling on hard rock mostly fragmented upon impact, ejecting cm-sized shards several tens of meters from the impact site. A few blocks fell on Ginostra village, seriously damaging a house, a road and a water tank (Fig. 4a). Eyewitness accounts report the fall of several blocks along the western flank of the volcano and in the sea in front of Ginostra at the beginning of Phase 2.

The distribution of the impact craters is strongly asymmetrical being concentrated in two narrow sectors with a 30–35° aperture oriented to the NE and WSW, respectively (Fig. 5a).

The largest block (~10 m^3) was encountered on the upper northeastern flank at an elevation of 450 m a.s.l. and a distance of 1 km from the craters. Upon impact and sliding the block formed a crater 18 m long and 8 m wide. Blocks of massive holocrystalline basaltic lava, lined with pumice layer of a few cebtimeters in thickness were concentrated northeast of the crater over an area of ~0.3 km^2. In contrast blocks which fell on the SW side of the volcano and on Ginostra lack this pumice coating and consist of variably altered lava and scoria.

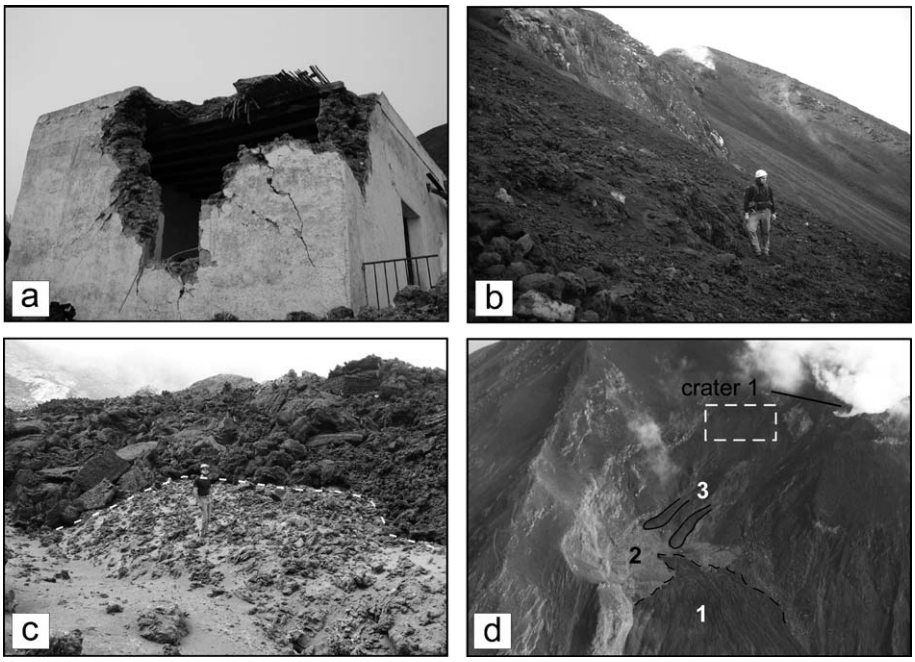

Fig. 4. Pictures of the deposits of the eruption. (a) House in Ginostra village damaged by m-sized block ejected during Phase 2. (b) Proximal fallout layer along the scarp connecting crater 1 to the Sciara del Fuoco. (c) Scoria flow deposit in active lava field partly covered by younger lava flows. Note ash covering the flow deposit. (d) Active lava flows (1) covering deposits of pyroclastic flows (2), photographed on April 18, 2003. Hot avalanche lobes (3) overlap the scoria flow deposit on northern side of the lava field. White box encloses proximal fallout area photographed in picture (b). Picture (a) is courtesy of K. Cashman.

4.3.2. Fallout tephra

The wind-blown fallout deposit from the convective plume consists of variably expanded and mingled pumice clasts and lithic fragments. It forms a continuous bed in the proximal area extending up to 0.6 km from the vent, reaching maximum thickness of 15 cm in the valley between the Pizzo Sopra la Fossa and the Vancori peaks (Fig. 5b). On the Vancori, the deposit has an average thickness of 2 cm, is very well sorted ($\sigma = 0.89$), mainly comprising coarse-grained lapilli ($Md\phi = -3.61$) and bearing a significant amount of ash finer than 1 mm (F1 = 4.34 wt.%). The juvenile component accounts for 63% by weight of the deposit (Fig. 6) and is partly composed of smooth, exceptionally expanded clasts bearing a large hollow cavity in its central part (constituting up to 70 vol.% of the clast).

The isomass map was drawn by interpolating measurements of mass loading per unit area made along three transects across the deposit at increasing distance from the craters and at scattered sites in proximal area (Fig. 5b).

A moderately sorted, incipiently welded spatter deposit was observed across the summit area of the volcano. In a site located 350 m NE of crater 1 this deposit was 1-m thick and consisted of dm-sized spatter fragments mixed with subordinate amounts of cm- to dm-size accidental lithic clasts (Fig. 4b). Individual juvenile clasts were flattened and elongated due to splashing upon landing and to limited downhill flowage immediately after landing. This deposit was likely emplaced from the dense, proximal fallout of the main jet formed during Phase 2.

4.3.3. Pyroclastic flow

A coarse-grained pyroclastic flow deposit was emplaced on top of the active lava flow field on the upper, eastern sector of the Sciara del Fuoco (Fig. 5c). The deposit was dispersed over an area of 0.025 km^2 with an estimate average thickness of 5 m (Figs. 4c and 5c). Field inspection made on May 13, 2003 revealed that most of the deposit was already covered by new lava that continued to be emitted following the paroxysm. However, limited portions of the deposit had been pushed upwards onto the surface of the lava field possibly as a result of lava inflation from below. Grain-size analysis of a 2-kg sample of the uplifted deposit indicates that the deposit matrix was poorly sorted ($\sigma = 2.16$), medium-

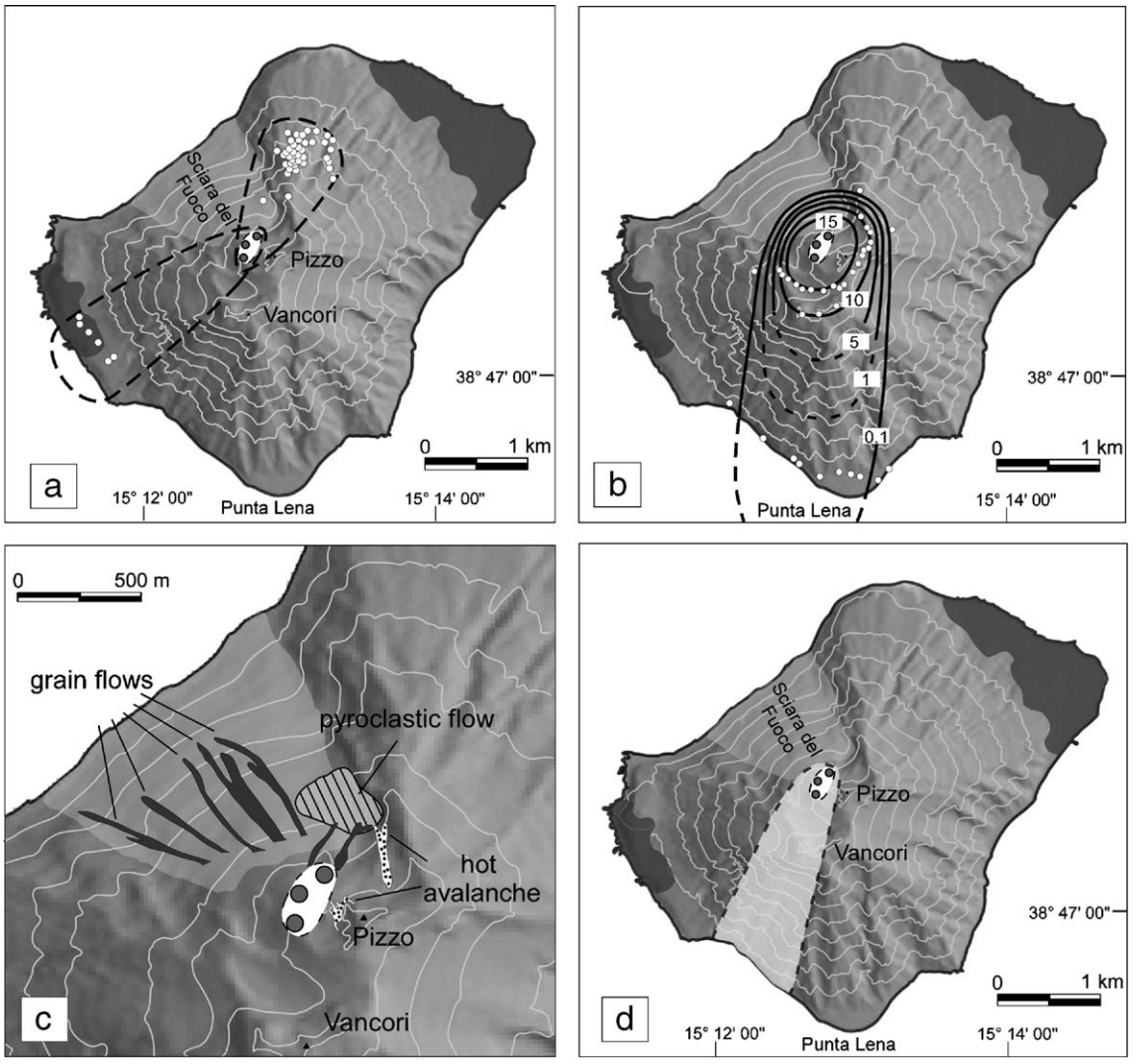

Fig. 5. (a) Mapped impact craters from larger ballistic blocks emitted during Phase 2. Dashed lines enclose the areas of higher concentration of blocks. Measurements of blocks and GPS locations of 16 impact craters were performed during field surveys made in April and May 2003. Impact craters produced by blocks with diameter ≥2 m were also mapped using data aerial photogrammetric surveys of the island (March 15, 2003, scale 1: 7000; April 16 scale 1: 8000 and May 26, 2003, scale 1: 5000) [16]. (b) Isomass map of fallout deposit. Values refer to kg/m^2. (c) Areal dispersion of grain flow (dark gray), hot avalanche (dottled area) and pyroclastic flow (striped area) deposits. (d) Dispersion of top ash layer.

coarse ash (Mdϕ=0.44), mainly composed by crystal-rich, vesicle-poor, scoria and subordinate pumice clasts (57 wt.%) (Fig. 6). The scoria flow deposit dispersion accords well with the source area of the ground hugging ash plume visible during Phase 3 in the photographic records.

4.3.4. Late ash and lapilli fallout

A 5-cm thick, red ash and lapilli bed overlies the pumice deposit about 300 m SSW of crater 3. A representative sample taken at this locality reveals that it was fine grained (F1=53.86 wt.%, Mdϕ=−0.10) and well sorted (σ=1.10). The deposit mainly bears altered lava fragments (79 wt.%) with subordinate amounts of fresh crystalline scoria fragments (Fig. 6). The dispersion and lithology of the bed matches the dispersion direction and color of the short-lived plume emitted during Phase 4 (Fig. 5d).

4.3.5. Secondary flows

Hot avalanche deposits resulted from sliding and secondary mass flowage of fall deposits accumulated on

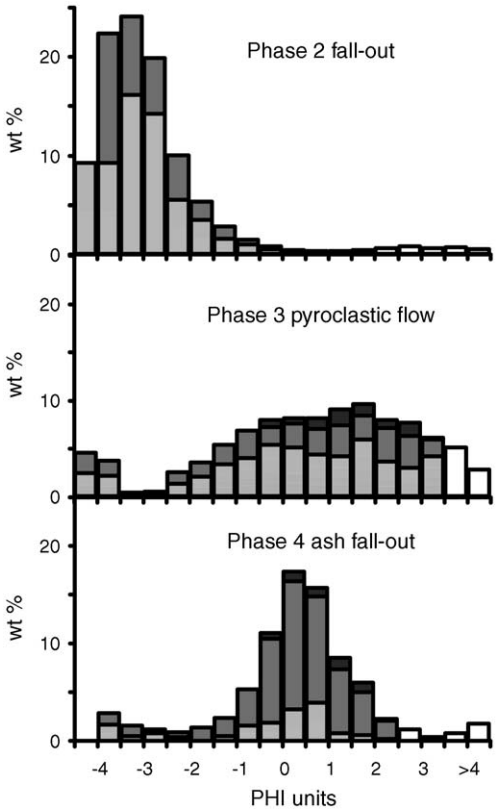

Fig. 6. Granulometric distribution of representative samples from eruptive Phase 2 (fallout lapilli layer sampled at Vancori), Phase 3 (pyroclastic flow sampled on lava field) and Phase 4 (ash layer sampled between Pizzo and Vancori). Black, dark gray and light gray bars indicate weight percentage of crystals, lithics and juvenile fragments, respectively.

steep slopes. This occurred locally around the crater area (Fig. 5c). The main deposit is a 4-m wide, 3-m thick and a few tens of meters long, steep sided lobe that accumulated on the southern edge of the lava field. Observations made by helicopter in the days after the event, followed by field inspections, showed that the deposit originated from the sliding of the spatter agglutinate deposit about 300 m upslope of the accumulation site (Fig. 5d).

5. Eruption dynamics

5.1. Phase 1

The paroxysm was preceded by a short precursory emission apparent from a temperature increase at the summit craters. In addition inflation of the summit cones occurred due to pressurization of the shallow conduits at 7:12:33 GMT [10,13]. The onset of deformation thus occurred 34 s before initial ash emission recorded by the IR-thermometer.

The eruption started at 7:13:07 GMT with initial ash emission from all three summit craters. The ash emission could be due to early gas leakage and/or sliding of the crater walls induced by the rapid ground deformation. Whatever the cause of this initial ash emission, the mass of ejected products during this phase with respect to the total erupted mass was trivial.

5.2. Phase 2

Our data indicate an abrupt temperature increase starting at 7:13:19 GMT in the IR log. This coincided with the formation of a compression wave, a vertical jet above the craters, and the emission of a large number of blocks and bombs. A convective column extending to a height of ~4 km formed above the craters in the following minutes eventually feeding a plume that dispersed southwards. The initial jet was sustained for just 11 s and was then followed by a 9-s long series of shorter explosions recorded as a sequence of spikes in the thermal log.

Field data indicate that most of the pyroclastic material was emitted during this phase. Loading per unit area of fallout deposit vs. isomass area plot indicates a single exponential decay law. Total erupted mass calculated according to [18], yielded values of 1.1–1.4×10^8 kg, considering a maximum error of 10%. The average mass discharge rate obtained using a total duration of 39 s for this phase as defined by thermal log is thus 2.8–3.6×10^6 kg/s. Assuming that most of the material was emitted during the initial 10 s (onset time of the main thermal peak) indicates that the discharge rate possibly peaked at 1.0–1.2×10^7 kg/s. These values correspond to a magma discharge rate of 2.3–2.9×10^6 kg/s and 8.1–9.7×10^6 kg/s (DRE = 2850 kg/m^3 and juvenile/lithic ratio = 4.3). Mass flux has also been calculated during an explosive event from infrasonic data [19]. However, we are unable to do this because our infrasonic sensors were destroyed shortly after the event began.

The ejection of a large mass of crystal-poor pumice suggests that the eruption involved a magma batch compositionally different to the degassed, crystal-rich magma that was feeding the on-going lava flow.

5.3. Phase 3

At 7:13:59 GMT the beginning of a cluster of thermal spikes marked the onset of Phase 3. This phase was coincident with the formation of a scoria flow that

spread onto the lava field and the concurrent rise of a phoenix plume behind the Bastimento ridge.

The volume of the flow deposit, calculated from integrating average thickness over its aerial distribution, with an estimated error of 10%, is $0.9–1.1\times10^4$ m^3. Taking the total duration of Phase 3 (42 s) with a deposit density of 1200 kg/m^3, we obtain a time-averaged mass discharge rate during this phase of 2.5–3.1 10^5 kg/s. The magnitude and intensity of Phase 3 was thus significantly lower than Phase 2.

The images are not conclusive in assessing the source of the scoria flow; it could have originated at the summit craters after the main explosions (Phase 2) by boiling over activity, which eventually caused the flow to pour northeastwards through a low point at that end of crater 1. However, this hypothesis is in conflict with three observations. First, there is an absence, in aerial pictures taken immediately after the event, of fresh ash in the sector connecting the crater 1 rim to the lava field. Second, we find a different juvenile componentry for the scoria flow deposit when compared to that of the Phase 2 fallout deposit. The juvenile fragments of the flow deposit mainly consist of crystal-rich scoria formed by the same magma feeding the lava flow. Third, the presence in the IR-thermometer record of a distinct signal formed by a series of sharp, discrete thermal pulses (spikes) do not support the assumption of lower velocity, more sustained boiling over activity. These lines of evidence are more consistent with explosive activity that occurred from a vent(s) located at the southern edge of the lava field, along the same eruptive fracture that was feeding the on-going lava flow.

In our reconstruction, Phase 3 was thus caused by the rise of slug(s) along the same dyke feeding the lava flow. This caused a series of laterally directed explosions from a vent(s) located onto the lava field.

5.4. Phase 4

The final, waning phase of the eruption consisted of discrete, mild explosions mainly occurring at crater 3. The ejected tephra consisted of lithic fragments with subordinate amounts of crystal-rich scoria fragments and a negligible (<5 wt.%) content of pumice clasts. This suggests that this activity was related to the emission of small volume gas pockets with only minor involvement of deep magma.

The onset of Phase 4 can not be defined using the thermal log, because activity at the summit craters was not detectable by the thermal sensors until the phoenix plume and the vapor cloud from the hot avalanching on the lava field cleared.

The eruption ended at 7:20:54 GMT when the last thermal peak was recorded, giving a total duration of about 8 min.

5.5. Calculation of muzzle velocities of Phase 2

Because no direct measurements of the ballistic trajectories were available, we calculated ejection velocities for the blocks through a number of different approaches using both field and geophysical data.

5.5.1. Ballistic ejecta

The zone of maximum concentration of blocks is located between 750 and 1350 m NE of the crater area. The eruption movie and images revealed that most of the blocks landed within the first 30 s after the main explosion. Following [20], this is consistent with minimum launch velocities of 150 m/s and ejection angles ranging from 70° to 85°, with maximum heights of about 1050 m above the craters.

5.5.2. Seismic and thermal onset delay

Three out of four stations located at the summit at distances ranging from 250 to 600 m from the craters survived the explosions, transmitting seismic, thermal and acoustic data recorded within the explosion itself. Seismic signals were clipped but provided useful constraints on the timing of the explosive dynamics. In particular, the seismic signal went out of scale when an $\sim1.5\times10^4$ kg block landed ~20 m from the station, on the side of the Bastimento ridge facing away from the craters. This tare occurred 34.8 s after the thermal onset of Phase 2. Assuming this time as the time of flight of the block, its ballistic trajectory should be characterized by a launch angle of 86°, a maximum height of 1460 m above the craters and a velocity of 170 m/s. [20]. If the block had been launched any later, i.e. after the thermal onset of Phase 2, a lower launch angle and/or velocity is needed. However, quite a high launch angle is required to allow the block to land just over the Bastimento ridge as confirmed by the impact angle observed on the ground. This velocity is much higher than those measured for typical strombolian eruption at Stromboli ranging between 10 and 40 m/s [21–23].

Using this velocity (170 m/s), considering a stationary gas discharge regime and assuming that the fragments reach their terminal velocity in the conduit we have also calculated the gas velocity by trial and error using the Eq. (3) in [24] modified from [25]. The calculated gas velocity is 310 m/s.

Assuming that gas expansion, at least during the very first seconds of the explosion, was isothermal and that

the gas volume fraction was ~90%; we estimate a minimum gas overpressure of ~2.3 MPa. This value is more than one order of magnitude larger than the overpressure of about 0.2 MPa, estimated for the normal Strombolian activity [24,26].

5.5.3. Thermal log

A burst of high temperature material will rise through and increasingly fill the field of view (FOV) of the thermal sensor, so that the temperature will increase to reach a peak when the mixture has completely filled the FOV. Thus the time taken to reach a peak (dTe) can be used to approximate the time that it takes a burst of material to cover a known distance (HFOV), the vertical extent of the FOV, and the rise velocities of the emitted material can be simply calculated as HFOV/dTe.

Visual observations indicate that the plume emitted during Phases 1, 3 and 4 cannot be trusted to have ascended to the top of the FOV. For example, the plume emitted during the final event of Phase 4 was observed to blow obliquely away from the sensor, and thus it could be not have risen vertically. In these cases, we cannot apply this thermal approach. However, the materials of Phase 2 did certainly ascend approximately vertically and completely through the FOV. We also know, from the infrasonic array analysis, that the plume during Phase 2 was emitted by a source of known location (crater 1).

Using the sensor FOV diameter (~120 m), we calculated a velocity of 320 m/s for the first 18 s of Phase 2, declining to 40–100 m/s during the waning part of Phase 2. We believe that these velocities relate to the emission of a fast, leading ballistic jet and contrail, followed by a slower, expanding plume.

5.6. Depth of the fragmentation level

Although the infrasonic array was knocked out 50 s after the eruption onset, it did record the initial pressure signal. Infrasonic source location by array analysis indicates that the recording station ROC (Fig. 1) was at a distance of 460 m from the vent. At this distance and considering a sound speed in the atmosphere of 340 m/s the time delay between the thermal and the infrasonic onset should be of 1.35 s. However, infrasonic waves arrived 1.21 s after the thermal onset, i.e. 0.14 s (dt) before the expected arrival time. This time delay (dt) indicates that sound was generated inside the conduit when the fragments separated from the magma column and that was propagating at a speed faster that the gas cloud. We assumed that the sound speed inside the conduit (c) ranged between 710 and 440 m/s, calculated for air at 1000 °C and for an ash-rich vapor, respectively. Using these velocities and the estimated ascent velocity of 310 m/s (U) for the rising eruptive cloud we calculated the position $h = \mathrm{dt}^*(U^*c)/(U-c)$ [24,27] of the infrasonic source within the conduit. This indicates that the position of the fragmentation level inside the conduit was at a very shallow depth of ~77–146 m below the crater rim. This is roughly at the same level (600–670 m a.s.l.) as the sources of normal Strombolian activity at Stromboli.

6. Conclusions

Analysis and integration of visual, field and geophysical data collected during and after the April 5, 2003 paroxysmal explosion of Stromboli provide an outstanding opportunity to assess the dynamics of this eruption and make fundamental inferences regarding this style of explosive activity.

Thermal data allowed us to quantitatively document the event, revealing that the event consisted of a series of discrete explosive pulses. These, in turn, clustered into four separate phases. The average pulse frequency was 4.2 events/min, reaching a maximum during Phase 1–2 (11 events/min), and decreasing to 4 events/min in Phase 3 and to 2 events/min during late Phase 4.

Maximum energy release occurred during Phases 2 and 3 when most of the material was emitted. Phases 1 and 4 represented, respectively, a short precursory emission and the waning tail of the event. The progressive increase of lithic/juvenile ratio from Phase 2 to Phase 4 suggests that the early phases were characterized by substantial fragmentation of magmatic material, whereas gas bursting essentially drove the late phase.

Independent calculation methods indicate that gas velocities during Phase 2 peaked at 310–320 m/s when large blocks were ejected at velocities of up to 170 m/s. The integrated geophysical component of the data set indicates that the overpressure needed to accelerate gas and blocks to the this value is in the range of 2.5 MPa and is consistent with the sudden failure of a pressurized container located about 120 m below the crater rim.

The average mass discharge rate attained 2.8–3.6×10^6 kg/s for a total duration of 39 s with a possible peak during the main pulse at $1.0–1.2\times10^7$ kg/s. We used the method developed by [28] to check the compatibility between observed column height and calculated magma discharge rate. Assuming a magma temperature of 1100 °C, an efficiency factor of heat usage of 0.5 and magma specific heat content of 1.1×10^3 J/kg K, the calculated magma discharge rates

correspond to theoretical column heights ranging from 3650 to 3950 m, in agreement with the observed value of ~4000 m.

Assuming a gas volume fraction of 90%, eruption through a single shallow conduit and using the peak volume discharge rate ($1.1–1.4\times10^4$ m^3/s) with the calculated gas and particle velocities, a diameter of ~30 m is obtained. However, the asymmetrical distribution and different nature of lithic blocks (altered scoria and vesicular lava SW of crater 3, and fresh, holocrystalline lava NE of crater 1) and visual observation of the explosion [10] indicate the activation of at least two vents.

Phase 3 began about 40 s after the start of Phase 2 from a vent located in the higher portion of the Sciara del Fuoco, where lava emission was in progress. This event discharged material onto the active lava flow field, with an average mass flux of $2.5–3.1\times10^5$ kg/s, about one order of magnitude lower than during climactic phase.

Previous authors [10] suggested that the explosivity could be partly produced by magma–water interaction related to shallow water accumulation during heavy rainfall on the day before the eruption and that crater clogging due to accumulation of debris was fundamental in determining the dynamics of the explosion. We believe that, although it is not possible to exclude completely water involvement, the features of the juvenile products (high vesicularity, low viscosity at the time of landing, high temperatures in proximal deposits determining welding) suggest that magmatic volatiles drove the explosivity of the April 5 event. Authors [29] have underscored that the triggering mechanism of the April 5 event was initiated at a pressure > 240 MPa and was related to the ascent of a volatile-rich melt (H_2O = 2–2.5 wt.%, CO_2 = 1300–1800 ppm). This nearly aphyric, bubble-rich magma blob rapidly rose through and interacted with the shallow crystal-rich magma just before the eruption resulting in the ejection of mingled material. The high explosivity is related to an excess of pressure (2.5 MPa) due to incomplete equilibration of the magmatic foam 'diapire' during its rapid ascent [30].

The occurrence of two main bursts of activity (Phases 2 and 3) is here interpreted as a result of the splitting of the gas–magma pocket between the main vertical conduit system and the lateral dyke which at that time was feeding the lava flow. The delayed explosion of Phase 3 and the reduced mass of ejected material is accounted for by the narrower size and inclination of this lateral pathway as compared to the main conduits.

The emitted products, impulsive nature of the event, and eruptive dynamics make the explosion of April 5, 2003 fully comparable with other historical paroxysms of Stromboli volcano. Paroxysmal explosions are usually associated with the formation of sudden, window-breaking, compressive waves described by witnesses as single or repeated 'cannon shots' [31,32] and ejection of m-sized blocks and bombs to a few kilometers. Block fallout mainly affects the NNE and SW sectors of the island, mirroring the elongate geometry of the crater area [3,5,33].

The best-documented historical paroxysm, the 1930 event, was described in detail by [5]. It had striking similarities with the April 5 explosion, both in terms of eruptive dynamics and type and distribution of products. The 1930 eruption suddenly started interrupting 'normal' Strombolian activity with mild explosions emitting ash, followed by a main explosive phase emitting spatter and pumice bombs and launching lithic blocks that fell on the SW and NNE flanks. The end of the 1930 paroxysm was marked by ash-rich explosions and lava emission from the summit craters. As a whole these features suggest that whatever the conditions of the uppermost part of the feeding system the overall eruptive dynamics is not significantly modified. These conditions were open vents in 1930 (as well as in 1916 and 1919 events) and debris-clogged vents and lava effusion during April 5 [5,33,34]. In addition, emission of crystal-poor, highly vesicular pumice during exceptionally violent explosions, has been documented in many papers [5,33]. This strongly suggests that this type of explosive activity at Stromboli is accounted for by the same mechanism as proposed for the April 5, 2003 event.

Acknowledgments

This work was supported by GVN DPC program. A. Harris was also supported by NSF grant EAR-0207734. The Italian Civil Protection is acknowledged for logistic support and helicopter use during field activities. The research strongly benefited from photographic and video data acquired and generously provided by S. Calvari and P. Scarlato. A. Franssen, N. Casagli, S. Ballarò are acknowledged for having kindly shared further photographic material. M. Marsella provided aerial pictures and technical support for mapping of ballistic blocks. The volcanological guides of Stromboli Island and the Guardia di Finanza alpine guides are acknowledged for having provided fundamental support during field activities throughout and after the 2002–2003 eruptive crisis. K. Cashman is acknowledged for

fruitful discussions and having kindly shared some field pictures with the authors. This paper benefited from accurate and fruitful revisions by J.C. Tanguy and an anonymous reviewer.

References

[1] A. Tibaldi, Multiple sector collapses at Stromboli volcano, Italy: how they work, Bull. Volcanol. 63 (2001) 112–125.
[2] M. Rosi, A. Betagnini, P. Landi, Onset of the persistent activity at Stromboli volcano (Italy), Bull. Volcanol. 62 (2000) 294–300.
[3] F. Barberi, M. Rosi, A. Sodi, Volcanic hazard assessment at Stromboli volcano based on review of historical data, Acta Vulcanol. 3 (1993) 173–187.
[4] G. Mercalli, I vulcani attivi della Terra, Hoepli, Milan, 1907.
[5] A. Rittmann, Der Ausbruch des Stromboli am 11 September 1930, Zeits Vulkanol. 14 (1931) 47–77.
[6] A. Bonaccorso, S. Calvari, G. Garfì, L. Lodato, D. Patanè, Dynamics of the December 2002 flank failure and tsunami at Stromboli volcano inferred by volcanological and geophysical observations, Geophys. Res. Lett. 30 (2003), doi:10.1029/2003GL017702.
[7] P. Tommasi, F.L. Chiocci, M. Marsella, M. Coltelli, M. Pompilio, Preliminary analysis of the December 2002 instability phenomena at Stromboli volcano, Abstract Volume from Meeting on Occurrence and Mechanisms of Flow-Like Landslides in Natural Slopes and Earthfills, Sorrento, Italy, 2004, pp. 297–303.
[8] S. Tinti, G. Pagnoni, F. Zaniboni, Tsunami generation in Stromboli Island and impact on the south-east Tyrrhenian coasts, Nat. Hazards Earth Syst. Sci. 3 (2003) 299–309.
[9] M. Ripepe, E. Marchetti, G. Ulivieri, A. Harris, J. Dehn, M. Burton, T. Caltabiano, G. Salerno, Effusive to explosive transition during the 2003 eruption of Stromboli Volcano, Geol. Soc. Amer. Bull. 33 (2005) 341–344.
[10] S. Calvari, L. Spampinatoi, L. Lodato, The 5 April vulcanian paroxysmal explosion at Stromboli volcano (Italy) from field observation and thermal data, J. Volcanol. Geotherm. Res. 149 (2006) 160–175.
[11] M.L. Carapezza, S. Inguaggiato, L. Brusca, M. Longo, Geochemical precursors of the activity of an open conduit volcano: the Stromboli 2002–2003 eruptive events, Geophys. Res. Lett. 31 (2004), doi:10.1029/2004GL019614.
[12] A. Aiuppa, C. Federico, Anomalous magmatic degassing prior to the 5th April 2003 paroxysm on Stromboli, Geophys. Res. Lett. 31 (2004), doi:10.1029/2004GL020458.
[13] M. Mattia, M. Rossi, F. Guglielmino, M. Aloisi, Y. Bock, The shallow plumbing system of Stromboli island imaged from 1 Hz instantaneous GPS positions, Geophys. Res. Lett. 31 (2004), doi:10.1029/2004GL021281.
[14] M. Ripepe, E. Marchetti, P. Poggi, A. Harris, A. Fiaschi, G. Ulivieri, Seismic, acoustic, and thermal network monitors the 2003 eruption of Stromboli Volcano, Eos, Trans.-Am. Geophys. Union 85 (2004) 329–332.
[15] A. Harris, D. Pirie, K. Horton, H. Garbeil, E. Pilger, H. Ramm, R. Hoblitt, C. Thornber, M. Ripepe, E. Marchetti, P. Poggi, DUCKS: low cost thermal monitoring units for near-vent deployment, J. Volcanol. Geotherm. Res. 143 (2005), doi:10.1016/j.jvolgeores.2004.12.007.
[16] A.J.L. Harris, D.S. Stevenson, Thermal observations of degassing open conduits and fumaroles at Stromboli and Vulcano using remotely sensed data, J. Volcanol. Geotherm. Res. 76 (1997) 175–198.
[17] P. Baldi, F. Belloli, M. Fabris, M. Marsella, R. Monticelli, V. Signoretto, La fotogrammetria digitale differenziale per il monitoraggio del versante della Sciara del Fuoco (Isola di Stromboli) dopo l'evento del 30 dicembre 2002. 7 National ASITA meeting Verona, Italy, 2003.
[18] D.M. Pyle, The thickness, volume and grainsize of tephra fall deposits, Bull. Volcanol. 51 (1989) 1–15.
[19] S. Vergniolle, M. Boichu, J. Caplan-Auerbach, Acoustic measurements of the 1999 basaltic eruption of Shishaldin volcano, Alaska 1. Origin of Strombolian activity, J. Volcanol. Geotherm. Res. 137 (2004) 109–139.
[20] L.G. Mastin, A simple calculator of ballistic trajectories for blocks ejected during volcanic eruptions. U.S. Geological Survey open file report 01–45 (1991).
[21] M. Ripepe, M. Rossi, G. Saccorotti, Image processing of explosive activity at Stromboli, J. Volcanol. Geotherm. Res. 54 (1993) 335–351.
[22] E.A. Blackburn, L. Wilson, R.S.J. Sparks, Mechanism and dynamics of strombolian activity, J. Geol. Soc. (Lond.) 132 (1976) 429–440.
[23] B. Chouet, N. Hamisevicz, T.R. McGetchin, Photoballistic of volcanic jet activity at Stromboly, Italy, J. Geophys. Res. 79 (1974) 4961–4976.
[24] M. Ripepe, S. Ciliberto, M. Della Schiava, Time constraints for modelling source dynamics of volcanic explosions at Stromboli, J. Geophys. Res. 106 (2001) 8713–8727.
[25] G.S. Steinberg, J.I. Babenko, Experimental velocity and density determination of volcanic gases during eruption, J. Volcanol. Geotherm. Res. 3 (1978) 89–98.
[26] S. Vergniolle, G. Brandeis, Strombolian explosions: 1. A large bubble breaking at the surface of a lava column as a source of sound, J. Geophys. Res. 101 (1996) 20433–20447.
[27] M. Ripepe, A.J.L. Harris, R. Carniel, Thermal, seismic and infrasonic insights into conduit process at Stromboli volcano, J. Volcanol. Geotherm. Res. 118 (2002) 285–297.
[28] L. Wilson, R.S.J. Sparks, T.C. Huang, N.D. Watkins, The control of Volcanic column heights by eruption energetics and dynamics, J. Geophys. Res. 83 (1978) 1829–1835.
[29] N. Métrich, A. Bertagnini, P. Landi, M. Rosi, O. Belhadj, Triggering mechanism at the origin of paroxysm at Stromboli (Aeolian Archipelago, Italy): the 5 April.
[30] A. Bertagnini, N. Métrich, P. Landi, M. Rosi, Stromboli volcano (Aeolian Archipelago, Italy): an open window on the deep-feeling system of a steady state basaltic volcano, J. Geophys. Res. 108 (2003) 1–15.
[31] A. Riccò, G. Mercalli, Sopra il periodo eruttivo dello Stromboli cominciato il 24 Giugno 1891, Ann. Uff. Cent. Meteorol. Geodin. Ital. 11 (1892) 189–221.
[32] O. De Fiore, I fenomeni eruttivi avvenuti allo Stromboli dal 1914 al 1916, Boll. Soc. Sismol. Ital. 24 (1923) 9–66.
[33] G. Ponte, La catastrofica esplosione dello Stromboli, R. Accad. Naz. Lincei 28 (1919) 89–94.
[34] G. Ponte, La formidabile esplosione dello Stromboli del 1916, Mem. R. Com. Geol. It. 7 (1921) 1–34.